In-situ SAXS observation on metal-salt-derived alumina sol-gel system accompanied by phase separation

Yasuaki Tokudome, Kazuki Nakanishi,* Kazuyoshi Kanamori and Teiichi Hanada

Department of Chemistry, Graduate School of Science, Kyoto University, Kitashirakawa, Sakyo-ku, Kyoto 606-8502, Japan

*To whom correspondence should be addressed: E-mail: kazuki@kuchem.kyoto-u.ac.jp. Tel&Fax: +81-75-753-2925.

ABSTRACT

The structure formation process of hierarchically porous alumina gels has been investigated by in-situ small angle X-ray scattering (SAXS). The measurement was performed on the sol-gel solution containing aluminum chloride hexahydrate ($AlCl_3 \cdot 6H_2O$), poly(ethylene oxide) (PEO), and propylene oxide (PO). The temporal divergence of scattering intensity in the low q regime was observed in the early stage of reaction, indicating that the occurrence of spinodal-decomposition-type phase separation. Detailed analysis of the SAXS profiles revealed that phase separation occurs between weakly branched polymerizing aluminum hydroxide (AH) and PEO. Further progress of the condensation reaction forms phase-separated two phases, that is, AH-rich phase and PEO-rich phase with the micrometer-range heterogeneity. The growth and aggregation of primary particles occurs in the phase-separated AH-rich domain, and therefore, the addition of PEO influences on the structure in nanometer regime as well as micrometer regime. The moderate stability of oligomeric species allows

homogeneous condensation reaction parallel to phase separation and successful formation of hierarchically porous alumina gel.

KEYWORDS: SAXS, alumina, macroporous, mesoporous, phase separation, monolith, sol-gel

1. Introduction

Monolithic porous materials possess various benefits arising from its structural features, and have drawn considerable attention especially in the fields where a liquid phase reaction is involved [1,2]. As well as the considerable mechanical strength and thermal shock resistance, these materials afford thin wall (low concentration of solid phase) and high porosity compared to particle-packed bed, resulting in very low resistance to fluid flow and hence low pressure drop [3]. The lower pressure drop allows high speed operations without requiring additional energy consumption. Moreover, a desirable structure which is suitable for an intended application can be flexibly designed owing to the widely controllable porosity and pore size. In fact, not a few reports have proven that monolithic porous materials show high reaction efficiency as a whole system when being employed in the fields of catalysis and separation [4−9].

Phase separation accompanied by sol-gel transition is one of the promising methodologies established for monolithic porous silica [10]. By controlling the miscibility between alkoxy-derived condensates and solvent (additives are also included in some cases), phase separation can be induced in parallel with the sol-gel transition, which freezes the transient phase-separated structures and produces various morphologies with micrometer-range heterogeneity. Further progress of polycondensation forms distinct phase-separated two phases, i.e., gel-rich and fluid-rich phases, and various porous structures in micrometer regime are obtained after removal of the fluid-rich phase. The silica gel thus obtained shows high efficiency as a separation column for liquid chromatography [5,11]. However, it

has still been an appreciable challenge to extend the synthesis route to diverse sol-gel systems because most metal alkoxides, such as transitional metal alkoxides, are highly reactive and are not stable in an aqueous solvent. Although the employment of chelating agents and strong acids are successful strategies for controlling the hydrolysis and polycondensation reactions, the too-high reactivity also causes the serious problem. The problem is that metal alkoxides in some cases are highly expensive or commercially unavailable [12−14].

Recently, we have reported the alternative route which would overcome these problems by using metal salts as an inorganic precursor. Monolithic alumina with tailored macropores can be synthesized from aluminum chloride hexahydrate ($AlCl_3 \cdot 6H_2O$) and poly(ethylene oxide) (PEO) dissolved in an aqueous solvent, followed by the addition of propylene oxide (PO) [15]. This synthesis route is potentially applicable not only to transitional metal oxide but also to mixed metal oxides and metal phosphates, because the mixing of multiple metal salts is readily achieved even in the case that concentration of metal salts are relatively high. Actually, the synthesis of macroporous materials was successfully demonstrated in yttrium aluminum garnet ($Y_3Al_5O_{12}$) and dicalcium phosphate anhydrous ($CaHPO_4$) systems [16,17].

Despite its considerable importance, the structure formation process of inorganic gels in the above-mentioned metal-salt-derived sol-gel systems has not been demonstrated and information during the reaction is scarce. In this contribution, we have employed an in-situ small angle X-ray scattering (SAXS) technique to investigate the structure formation process of alumina gel. In-situ SAXS is suitable technique for the analysis of structures in the nanometer scale corresponding to primary particles and aggregates in the domains undergoing phase separation during the reaction. Although small angle light scattering (SALS) is also a well-known approach for the structural evolution of phase-separated domains, the size scale of interest in this study is much smaller, and hence we adopt in situ SAXS for characterization. The better knowledge of the structure formation process of alumina gels would allow a better design of well-defined macro- and mesoporous structures with highly

controlled surface properties. Additionally, the perception in the structure formation process in the alumina system would give a valuable guide to other metal-salt-derived sol-gel systems, including transition metal oxides, mixed metal oxides, and phosphates. The feasibility of the present reaction is defined by the size and structure of polymerizable species in the early stage of the reaction, and hence, understanding of the structure formation process of porous alumina gel provides definitive clues to morphology control in the diverse sol-gel systems which involve metal salts and additive polymers.

2. Experimental

2.1 Materials

Aluminum chloride hexahydrate ($AlCl_3 \cdot 6H_2O$: Aldrich, 99%) was used as an aluminum source, and a mixture of distilled water and ethanol (EtOH: Kishida Chemical, 99.5%) as solvent. Propylene oxide (PO: Aldrich, ≥ 99%) was added to initiate the condensation reaction, and poly(ethylene oxide) (PEO: Aldrich) with viscosity averaged molecular weight (M_v) of 1,000,000 was used as a polymer for inducing phase separation. All reagents were used as received.

2.2 Synthesis and Characterization

First, 4.32 g of $AlCl_3 \cdot 6H_2O$ and w_{PEO} g of PEO (w_{PEO}= 0 or 0.07 g) were dissolved in a mixture of 6.00 g of distilled H_2O and 2.77 g of EtOH. Then, under the ambient condition (25 °C), 3.11 g of propylene oxide was added. After being stirred for 1 min, the resultant homogeneous solution was injected into copper vessel with a polyimide window, sealed and kept at 40 °C for the in-situ SAXS measurement. The SAXS measurement was carried out at BL40B2 at SPring-8 using the incident synchrotron X-ray with the wavelength, λ, of 0.10 nm. Scattered X-ray was detected by an imaging plate (IP, R-AXIS VII, Rigaku Corp., Japan) under the accumulation time of 45 s on each measurement point. The instrument was operated with a sample-to-detector distance of 1649.08 mm. After the background was subtracted, the scattering profiles were circular-averaged and plotted against the scattering vector, q, according to the following relation:

$$q = (4\pi / \lambda)\sin\theta \qquad (1)$$

Where the 2θ is scattering angle. On the other hand, the rest of the injected samples were also reacted in a closed glass vessel for the purpose of the synthesis of bulk alumina gels. After gelation, the wet gel was aged for 24 h at 40 °C. Subsequently, the wet gels were subjected to solvent exchange with 2-propanol at 60 °C. Supercritical drying was carried out in a custom-built autoclave (Mitsubishi Material Techno Corp., Japan) using supercritical carbon dioxide at 80 °C and 14.0 MPa, yielding aerogels that preserved the dimensions of the corresponding wet gel. The morphologies of synthesized aerogels were observed with a scanning electron microscope (SEM: JSM-6060, JEOL Ltd, Japan, with a Pt-Pd coating). Micro-mesoporous characters of aerogels were investigated by a N_2 adsorption-desorption apparatus (BELSORP-mini II, Bel Japan Inc., Japan). Before each measurement, the sample was outgassed under vacuum at 200 °C.

3. Results and Discussion

Utilization of propylene oxide as a proton scavenger was first reported by Itoh et al. in silica-alumina sol-gel system, where tetraethoxysilane (TEOS) and $AlCl_3 \cdot 6H_2O$ were used as silica source and sources, respectively [18]. Gash et al. further extended this method to the non alkoxy-derived sol-gel systems [19]. Using stable metal salts such as metal chlorides and nitrates as starting materials, the homogeneous gelation is triggered by the addition of epoxides and leads to the robust and monolithic metal oxide aerogels. Epoxides act as proton scavengers through protonation of the epoxide oxygen and subsequent ring-opening reactions brought about by the nucleophilic anionic conjugate base, such as H_2O or Cl^- [18,19]. The moderate and uniform increase in solution pH allows the homogeneous hydrolysis and condensation reactions to produce monolithic gels in various sol-gel systems including alumina [20]. In the previous report, we modified the above procedure and demonstrated the synthesis of hierarchically macro- and mesoporous alumina by the addition of PEO [15]. When an appropriate amount of PEO is included in the sol-gel system, phase separation and

sol-gel transition concur, which results in the formation of macropores and mesotextured alumina skeletons after the removal of the fluid-rich phase. Fig. 1 shows the SEM images of supercritically-dried gels prepared with (a) w_{PEO} = 0 g and (b) w_{PEO} = 0.07 g. Without the addition of PEO, no structure was formed in micrometer range [part (a)], and the appearance of monolithic gel was translucent. On the other hand, the addition of PEO induced phase separation in parallel with the sol-gel transition, and an opaque gel with structure in the micrometer range was obtained [part (b)]. The occurrence of phase separation is related to the miscibility of a polymeric system, which can be

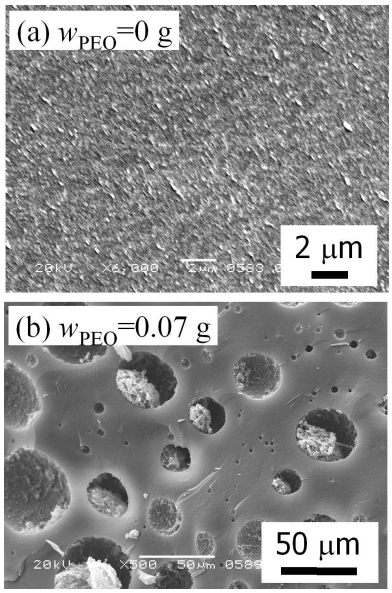

Fig. 1. Scanning electron microscope images of supercritically-dried samples prepared with (a) w_{PEO} = 0 g and (b) w_{PEO} = 0.07 g.

estimated by the Flory-Huggins formulation [21−23]. The Gibbs free energy change on mixing, ΔG, can be described as follows:

$$\Delta G \propto RT\left(\frac{\phi_1}{P_1}\ln\phi_1 + \frac{\phi_2}{P_2}\ln\phi_2 + \chi\phi_1\phi_2\right), \qquad (2)$$

where χ is the interaction parameter, ϕ_i and P_i are the volume fraction and the degree of polymerization of component i (i = 1 or 2), respectively, R is the gas constant, and T is the temperature. Volume fractions ϕ_1 and ϕ_2 are related with $\phi_1 + \phi_2 = 1$. The former two terms in parenthesis represent the

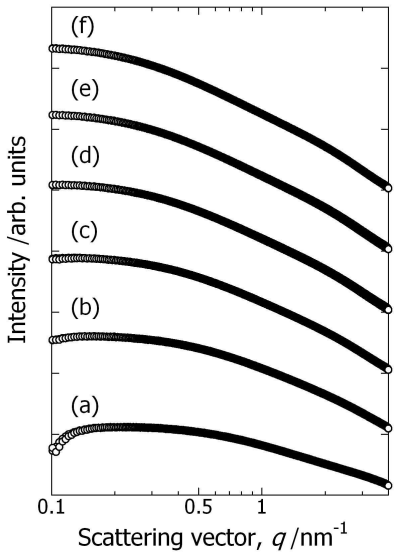

Fig. 2. Log-log plotted time evolution of SAXS profiles for the sample prepared with w_{PEO} = 0 g; (a) 208 s, (b) 508 s, (c) 808 s, (d) 1108 s, (e) 1408 s, (f) 1708 s after the addition of propylene oxide. The intensity is arbitrarily shifted for clarity. Gelation time was 1200 s.

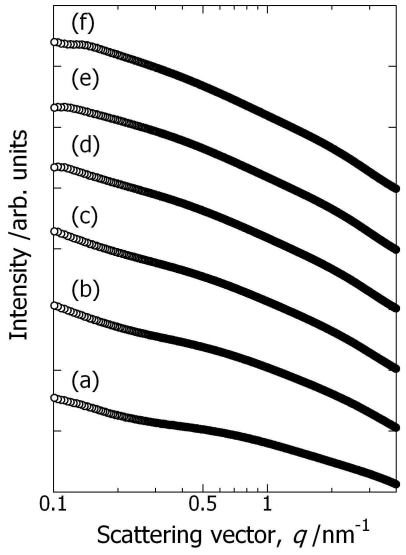

Fig. 3. Log-log plotted time evolution of SAXS profiles for the sample prepared with w_{PEO} = 0.07 g; (a) 245 s, (b) 540 s, (c) 840 s, (d) 1140 s, (e) 1440 s, (f) 1740 s after the addition of propylene oxide. The intensity is arbitrarily shifted for clarity. Gelation time was 1440 s.

entropic contribution, and the last term the enthalpic contribution. In the present alumina system, phase separation occurs due to the loss of mixing entropy [15]. Namely, either P_1 or P_2 in eq. (2) becomes large as a result of the homogeneous condensation reaction of aluminum hydroxide (AH) oligomers, which makes ΔG larger. Thus, the system phase-separates into AH-rich phase and PEO-rich phase during the condensation of hydrated aluminum species. Since the coexistent solvent is distributed in both phases, the present alumina system can be regard as a quasi-binary system, i.e., the AH-PEO system.

Figs. 2 and 3 represent the time evolution of SAXS profiles in double-logarithmic scale for samples prepared with w_{PEO} = 0 and w_{PEO} = 0.07 g, respectively. In the early stage of the reaction, a significant difference can be seen between the samples prepared with and without PEO. For the sample prepared with w_{PEO} = 0.07 g shown in Fig. 3, the scattering intensity steeply increases in the low q range before gelation. This phenomenon is closely related to the occurrence of

spinodal-decomposition-type phase separation. In the case of light scattering from an ideal binary polymer mixture, the inverse scattering intensity, $I^{-1}(q)$, can be written as follows [24]:

$$I^{-1}(q) = \frac{1}{\phi_1 g_D(P_1, q)} + \frac{1}{\phi_2 g_D(P_2, q)} - 2\chi, \qquad (3)$$

where χ is the interaction parameter, and $g_D(P_i, q)$ is the Debye function. When q approaches zero, the Debye function can be expanded into

$$g_D(P_i, q \to 0) = P_i\left(1 - \frac{1}{3}q^2 R_{Gi}^2\right) \qquad (qR_{Gi} < 1), \qquad (4)$$

where, R_{Gi} is radius of gyration of component i. On the other hand, second-order derivative of the Gibbs free energy change of mixing equals zero on a spinodal line in a phase diagram;

$$\frac{\partial^2 \Delta G}{\partial^2 \phi_1} = 0, \qquad (5)$$

Upon substituting eq. (2) into eq. (5), χ can be related to ϕ_i and P_i as

$$\frac{1}{P_1\phi_1} + \frac{1}{P_2\phi_2} = 2\chi, \qquad (6)$$

Consequently, if a system is on the spinodal line, scattering intensity in the low q limit can be described from eqs. (3), (4) and (6) as

$$\lim_{q \to 0} I^{-1}(q) = 0, \qquad (7)$$

This relation indicates that the scattering intensity in the low q limit increases and diverges when a system approaches and crosses the spinodal line, respectively. The present alumina sol-gel system can be regarded as a quasi-binary polymeric system, comprised of polymerizing AH and PEO, and therefore the discussion above would be also valid in this study. Thus, the divergence of scattering intensity in Fig. 3 before gelation signifies that the system crosses the spinodal line and thrusts into the spinodal region in the early stage of the reaction.

In order to analyze experimentally SAXS curves, we employed an unified equation proposed by Beaucage and Schaefer [25,26], which was developed to describe scattering from objects with a

hierarchical structure. The unified equation for the hierarchical structure with multiple structural levels is described as follows:

$$I(q) \approx \sum_{i=1}^{n} \left(G_i \exp\left(-q^2 R_{gi}^2 / 3\right) + B_i \exp\left(-q^2 R_{g(i+1)}^2 / 3\right) \left\{ \left[erf\left(qR_{gi} / 6^{1/2}\right) \right]^3 / q \right\}^{P_i} \right), \quad (8)$$

where n is the number of structure levels, R_{gi} is the radius of gyration of the ith level, P_i is the power-law exponent, G_i is the Guinier prefactor, and B_i is the prefactor specific to the type of power-law scattering falls. As an example, let us consider a hierarchical structure comprised of primary particles and aggregates [27]. The number of structure level, n, is two and we obtain four terms from eq. (8). Two terms with i = 1 corresponds to the contributions from larger particles, i.e., aggregates of primary particles, and R_{g1} and P_1 correspond to the radius of gyration and the power-law exponent of the aggregates, respectively. Also, the other two terms with i = 2 corresponds to the smaller particles, i.e., primary particles, and R_{g2} and P_2 correspond to the radius of gyration and the power-law exponent of the primary particles, respectively. Our previous report revealed that the supercritically-dried alumina gel prepared via the present synthesis route possesses two structural levels in the phase-separated AH domains; one corresponds to the primary particles, and the other the secondary aggregated particles, and

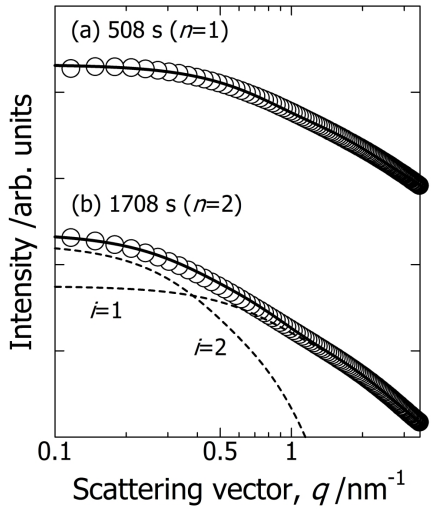

Fig. 4. Typical SAXS profiles (open circles) and fitting curves (solid lines) for the sample prepared without PEO. Fitted with (a) n=1 at 245 s and (b) n=2 at 1708 s. The dashed lines in (b) represent the individual contributions from i=1 and 2 terms in eq. (8).

hence, n = 2 [28]. However, it is reasonable to set n = 1 at the beginning of the reaction because the secondary particles form after the reaction proceeds to some extent. In this study, we first examined the fitting the SAXS curves with eq. (8) under the condition of n = 1, and if the fitting parameters, i.e., R_{g1} and P_1, were not convergent, then we tried the fitting with n = 2. Typical SAXS profiles and fitting curves for the sample prepared without PEO are shown in Fig. 4.

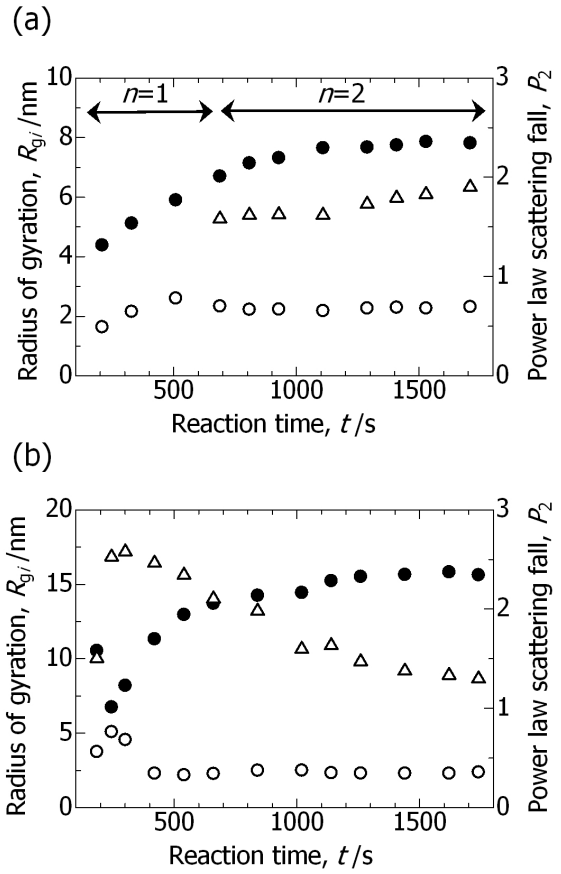

Fig. 5. Time evolutions of R_{g1}, R_{g2}, and P_2 for the samples prepared with (a) w_{PEO} = 0 g and (b) 0.07 g. Reaction time is defined as elapsed time from the addition of PO. Symbols represent following values, open circle: R_{g2}, open triangle: R_{g1}, closed circle: P_2.

Time evolutions of R_{g1}, R_{g2}, and P_2 for the samples prepared with w_{PEO} = 0 g and 0.07 g are plotted in Fig. 5. The SAXS curves for the sample prepared with w_{PEO} = 0 g could be fitted with n = 1 from the beginning of the reaction to 508 s [see Figs. 4(a)]. However, the fitting could not be preformed well at > 508 s [see Figs. 4(b)] because of the formation of the secondary particles. Therefore, the fitting with n = 2 was employed for the analysis of data from 508 s as shown in Fig. 5a.

For the sample prepared w_{PEO} = 0.07, on the other hand, the divergence of scattering intensity in the low q regime prevented the fitting with n = 1 even in the early stage of reaction. Hence, we performed the fitting with n = 2 for the total stage of reaction in this sample. Actually, it is highly unlikely that the secondary particles are formed just after the reaction starts. The values of R_{g1} are mainly derived from the divergence of scattering intensity, that is, the values of R_{g1} are not corresponding to the size of secondary particles and not physically meaningful in the early stage of reaction. The divergence of scattering intensity results in the appearance of maximum in R_g at 300 s for the PEO-incorporated system as observed in Fig. 5b. The appearance of the maximum in R_g was also observed in the initial stage of reaction in alkoxy-derived silica sol-gel system, where TEOS was utilized as silica source and PEO as phase separation inducer [29]. In Fig. 5, the values of R_{g2} at gelation point are a little smaller than those for aerogels (R_{g2} ~ 3.2 nm) [28]. Additionally, the values of P_2 at the gelation point, are 2.35 and 2.34 for the samples prepared with and without PEO, respectively, indicating that a primary particle has mass fractal dimension dissimilar to the case of the aerogel. Alumina aerogels prepared via the present synthesis route possess smooth surface with the surface fractal dimension of 4.0 [28]. These differences are presumably due to the progress of condensation and subsequent structural ordering during aging and drying processes. It has been reported that at moderate temperature, a highly acidic condition and/or a high Al concentration are favorable for the formation of alumina sols comprised of $Al_{13}O_4(OH)_{24}(H_2O)_{12}^{7+}$ (denoted as Al_{13}) [30−32]. The Al_{13} in alumina sols is well known to transform into aluminum hydroxides and forms a dense and packed structure during aging [32,33]. Considering the high Al concentration (Al_{total} = 1.08 mol/L) and the low pH (< 3) in the present study, the transformation from Al_{13} to aluminum hydroxide is likely to occur during aging and drying process, which accounts for the change in the fractal dimensions.

It is noteworthy in Fig. 5 that the values of R_{g2} are almost constant from the beginning of the reaction, while the values of P_2 become large with time. For the PEO-incorporated system, the copious polymeric species, having weakly branched structure (P_2 = 1.01, t = 245 s), are formed just after the PO

addition and those shape changes into more branched structure (P_2 = 2.06, t = 660 s). Subsequent particles growth into further ramified structure (P_2 = 2.34, t = 1740 s) and the simultaneous aggregation of primary particles result in the sol-gel transition. At the onset of the divergence of scattering intensity, polymeric species possess weakly branched structure, indicating phase separation occurs between PEO and the growing AH both of which are on average linear molecules in the early stage of the reaction. With an evolution of phase separation, Al polymeric species become concentrated in the phase-separated AH domain, which would bring about the progressive growth and aggregation of primary particles with increasing branches. This is manifested by the fact that P_2 for the sample prepared with w_{PEO} = 0.07 g changes more rapidly compared to that for the sample prepared without PEO. Based on the above discussion, the schematic illustrations of the structure formation process in PEO-incorporated system are represented in Fig. 6.

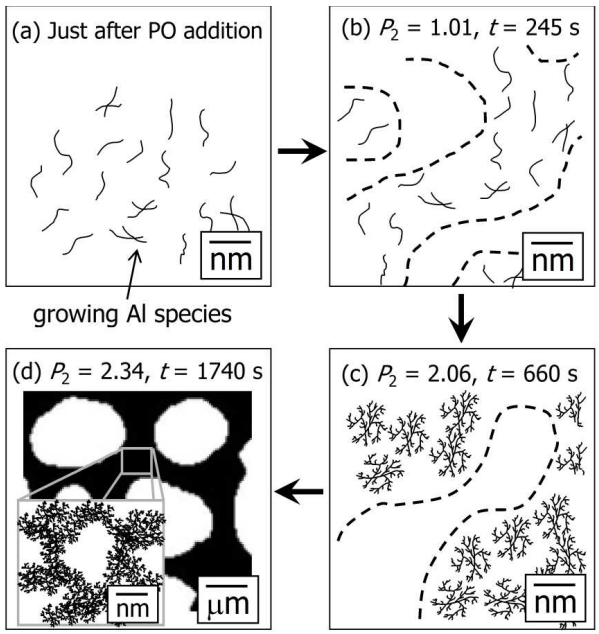

Fig. 6. The schematic illustrations of the structure formation process in PEO-incorporated system. The dashed line shows boundary of respective phase-separated domains. (a) a copious amount of oligomeric species are formed just after the PO addition, (b) phase separation occurs between PEO and the growing AH, (c) the growing AH become more branched and concentrated in the phase-separated AH domain, (d) the simultaneous growth and aggregation of primary particles (the growing AH) result in the sol-gel transition.

Fig. 7 shows the nitrogen adsorption-desorption isotherms and the corresponding pore size distribution curves for the supercritically-dried gels prepared with and without PEO. The addition of PEO decreases the mesopore volume as well as the mesopores size [28]. As discussed above, the present system can be regarded as the quasi-binary system and the phase separation occurs between AH and PEO, where the solvent is distributed in the both phases. The mesopores in the alumina skeletons are filled with solvent before being dried, and therefore, the decrease in mesopore volume indicates that the fraction of the solvent distributed in AH phase decreases with increasing PEO. The addition of PEO excludes the solvent from the AH domain, leading to the condensed Al polymeric species in AH domain and the formation of small mesopores.

The results obtained for the PEO-incorporated system in this study reveals that phase separation occurs in the early stage of the reaction where the primary particle is not a rigid particle but oligomeric

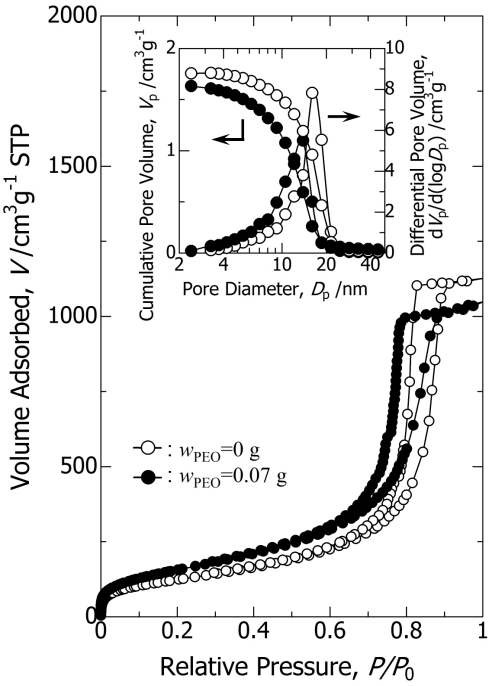

Fig. 7. Nitrogen adsorption-desorption isotherms of samples prepared with and without PEO. Inset shows the corresponding pore size distribution curves calculated by the BJH method using the adsorption branches. Symbols ○ and ● represent the data for the samples prepared with w_{PEO} = 0 g and w_{PEO} = 0.07 g, respectively.

species. The successful demonstration of the synthesis of porous alumina is presumably due to the moderate stability of oligomeric species because the instability of oligomeric species would result in the extensive growth of primary particles and the formation of precipitates rather than a monolithic gel. Thus, the inhibition of extensive growth of the primary particles is considerably important in the other sol-gel systems as well. In fact, we have pointed out the significance of size and number of primary particles in the Ca-P-O system [17]. The present study supports this fact more strongly by using in-situ SAXS measurements.

4. Conclusions

The structure formation process of hierarchically porous alumina gel has been investigated by in-situ SAXS measurement. The measurement was performed on the sol-gel solution containing $AlCl_3 \cdot 6H_2O$, PEO, and PO. A significant difference can be seen between the samples prepared with and without PEO. For the PEO-incorporated sample, the divergence of scattering intensity in the low q regime was observed in the early stage of reaction, indicating that spinodal-decomposition-type phase separation occurs in the presence of PEO. Detailed analysis of the SAXS profiles revealed that phase separation occurs between weakly branched polymerizing aluminum hydroxide (AH) (P_2 = 1.01, t = 245 s) and PEO. The growth and aggregation of primary particles occurs in the phase-separated AH-rich domain, and therefore, the addition of PEO influences on the structure in nanometer regime as well as micrometer regime. The moderate stability of oligomeric species allows homogeneous condensation reaction in parallel with phase separation and successful formation of hierarchically porous alumina gels. The inhibition of extensive growth of the primary particles is considerably important also for the synthesis of monolithic porous materials in other sol-gel systems from ionic precursors and epoxides.

ACKNOWLEDGMENT. The present work was supported by the Grant-in-Aid for Scientific Research (No. 21-607 for YT, No. 20350094 for KN, and No. 20750177 for KK) from the Ministry of

Education, Culture, Sports, Science and Technology (MEXT), Japan, and was partly supported by the Global COE Program “Integrated Materials Science” (No. B-09) of the MEXT, administrated by the Japan Society for the Promotion of Science (JSPS). The synchrotron radiation experiments were performed at the BL40B2 of the SPring-8 with the approval of the Japan Synchrotron Radiation Research Institute (JASRI) (Proposal No. 2007B1459). This work was partially carried out using facilities of Research Center for Low Temperature and Materials Sciences, Kyoto University.

REFERENCES

1. R. M. Heck, R. J. Farrauto, Catalytic Air Pollution Control: Commercial Technology, Wiley, New York, 1995.
2. F. Svec, J. M. J. Fréchet, Anal. Chem. 64 (1992) 820−822.
3. R. M. Heck, S. Gulati, R. J. Farrauto, Chem. Eng. J. 82 (2001) 149−156.
4. S. M. Fields, Anal. Chem. 68, (1996) 2709−2712.
5. H. Minakuchi, K. Nakanishi, N. Soga, N. Ishizuka, N. Tanaka, Anal. Chem. 68 (1996) 3498−3501.
6. H. Zou, X. Huang, M. Ye, Q. Luo, J. Chromatogr. A 954 (2002) 5−32.
7. M. P. Dudukovié, F. Larachi, P. L. Mills, Catal. Rev. – Sci. Eng. 44[1] (2002) 123−246.
8. C. Jas, A. Kirschning, Chem. Eur. J. 9 (2003) 5708−5723.
9. Y. Zhang, C. Y. Zhao, H. Liang, Y. Liu, Catal. Lett. 127 (2009) 339−347.
10. K. Nakanishi, J. Porous Mater. 4 (1997) 67−112.

11. N. Tanaka, H. Kobayashi, N. Ishizuka, H. Minakuchi, K. Nakanishi, K. Hosoya, T. Ikegami, J. Chromatogr. A 965 (2002) 35−49.

12. C. J. Brinker, G. W. Scherer, Sol–Gel Science: The Physics and Chemistry of Sol–Gel Processing, Academic Press, NewYork, 1990.

13. S. Doeuff, M. Henry, C. Sanchez, J. Livage, J. Non-Cryst. Solids 89 (1987) 206−216.

14. J. Livage, C. Sanchez, J. Non-Cryst. Solids 145 (1992) 11−19.

15. Y. Tokudome, K. Fujita, K. Nakanishi, K. Miura, K. Hirao, Chem. Mater. 19 (2007) 3393−3398.

16. Y. Tokudome, K. Fujita, K. Nakanishi, K. Kanamori, K. Miura, K. Hirao, T. Hanada, J. Ceram. Soc. Jpn. 115[2] (2007) 925−928.

17. Y. Tokudome, A. Miyasaka, K. Nakanishi, T. Hanada, J. Sol-Gel Sci. Techn. (in press).

18. H. Itoh, T. Tabata, M. Kokitsu, N. Okazaki, Y. Imizu, A. Tada, J. Ceram. Soc. Jpn. 101[9] (1993) 1081−1083.

19. A. E. Gash, T. M. Tillotson, J. H. Satcher, Jr., J. F. Poco, L. W. Hrubesh, R. L. Simpson, Chem. Mater. 13 (2001) 999−1007.

20. T. F. Baumann, A. E. Gash, S. C. Chinn, A. M. Sawvel, R. S. Mawell, J. H. Satcher, Jr., Chem. Mater. 17 (2005) 395−401.

21. P. J. Flory, J. Chem. Phys. 10 (1942) 51−61.

22. M. Huggins, J. Phys. Chem. 46 (1942) 151−158.

23. M. Huggins, J. Am. Chem. Soc. 64 (1942) 1712−1719.

24. P. G. De Gennes, Scaling Concepts in Polymer Physics, Cornell University Press, NewYork,

1979.

25. G. Beaucage, D. W. Schaefer, J. Non-Cryst. Solids 172 (1994) 797−805.

26. G. Beaucage, J. Appl. Cryst. 28 (1995) 717−728.

27. R. Wengeler, F. Wolf, N. Dingenouts, H. Nirschl, *Langmuir* 23 (2007) 4148−4154.

28. Y. Tokudome, K. Nakanishi, K. Kanamori, K. Fujita, H. Akamatsu, T. Hanada, J. Colloid Interface Sci. 338 (2009) 506−513.

29. R. Takahashi, K. Nakanishi, N. Soga, J. Sol-Gel Sci. Technol. 17 (2000) 7−18.

30. L. F. Nazar, L. C. Klein, J. Am. Ceram. Soc. 71 (1988) C85−C87.

31. J. Y. Bottero, J. M. Cases, F. Flessinger, J. E. Polrier, J. Phys. Chem. 84 (1980) 2933−2939.

32. J. Y. Bottero, M. Axelos, D. Tchoubar, J. M. Cases, J. J. Fripiat, F. Fiessinger, J. Colloid Interface Sci. 117 (1987) 47−57.

33. G. Fu, L. F. Nazar, A. D. Bain, Chem. Mater. 3 (1991) 602−610.

List of Figure Captions

Fig. 1. Scanning electron microscope images of supercritically-dried samples prepared with (a) w_{PEO} = 0 g and (b) w_{PEO} = 0.07 g.

Fig. 2. Log-log plotted time evolution of SAXS profiles for the sample prepared with w_{PEO} = 0 g; (a) 208 s, (b) 508 s, (c) 808 s, (d) 1108 s, (e) 1408 s, (f) 1708 s after the addition of propylene oxide. The intensity is arbitrarily shifted for clarity. Gelation time was 1200 s.

Fig. 3. Log-log plotted time evolution of SAXS profiles for the sample prepared with w_{PEO} = 0.07 g; (a)

245 s, (b) 540 s, (c) 840 s, (d) 1140 s, (e) 1440 s, (f) 1740 s after the addition of propylene oxide. The intensity is arbitrarily shifted for clarity. Gelation time was 1440 s.

Fig. 4. Typical SAXS profiles (open circles) and fitting curves (solid lines) for the sample prepared without PEO. Fitted with (a) n=1 at 245 s and (b) n=2 at 1708 s. The dashed lines in (b) represent the individual contributions from i=1 and 2 terms in eq. (8).

Fig. 5. Time evolutions of R_{g1}, R_{g2}, and P_2 for the samples prepared with (a) w_{PEO} = 0 g and (b) 0.07 g. Reaction time is defined as elapsed time from the addition of PO. Symbols represent following values, open circle: R_{g2}, open triangle: R_{g1}, closed circle: P_2.

Fig. 6. The schematic illustrations of the structure formation process in PEO-incorporated system. The dashed line shows boundary of respective phase-separated domains. (a) a copious amount of oligomeric species are formed just after the PO addition, (b) phase separation occurs between PEO and the growing AH, (c) the growing AH become more branched and concentrated in the phase-separated AH domain, (d) the simultaneous growth and aggregation of primary particles (the growing AH) result in the sol-gel transition.

Fig. 7. Nitrogen adsorption-desorption isotherms of samples prepared with and without PEO. Inset shows the corresponding pore size distribution curves calculated by the BJH method using the adsorption branches. Symbols ○ and ● represent the data for the samples prepared with w_{PEO} = 0 g and w_{PEO} = 0.07 g, respectively.